CHAPTER 2

Theory background and literature review

This chapter contains theory of ferroic materials, ferroelectric materials and their applications of temperature dependence behavior according to the phase transition of ferroelectric materials in ferroelectric phase to paraelectric phase structure, and magnetostriction properties or magnetic coupling electric properties in ferroelectric materials. The principle of Michelson interferometer for small displacement measurement, which is used to observe ferroelectric material strains induced by electric field, is also included.

2.1 Ferroic materials

Ferroic crystals are the crystals which have switched two or more domain orientation pattern to different pattern states when subjected to or affected by the external fields, such as mechanical stress (σ), electric field (E) or magnetic field (H), which result to orient the domain pattern states of spontaneous strain, spontaneous polarization and spontaneous magnetzation inside materials and so call ferroelastic, ferroelectric and ferromagnetic materials respectively [4]. The simple orientation pattern and hysteresis of domain are shown in Figures 2.1 and 2.2. In Figure 2.1, the ferroic orders are shown as ferroelectric which ferroelectric domain state is changed by interaction with the electric field, ferromagnetic which ferromagnetic domain state is changed by interaction with the magnetic field, ferrotoroidic (coupling of electric and magnetic properties) which domain state is changed by interaction with the electric and magnetic field, and ferroelastic which domain state is changed by interaction with the stress. In Figure 2.2, the characteristic hysteresis loop of ferroelectric, ferromagnetic and ferroelastic materials is illustrated when they are subjected to electric field, magnetic field and uniaxial stress, respectively, due to the reorientation of spontaneous domains. Ferroelectric effect is related to switching of local electric dipole by electric

field; ferromagnetic effect is related to change of magnetic dipole by magnetic field and the atomic displacement or strain is related to (change of) stress. Ferroelectric and ferromagnetic materials are commonly used in many applications such as capacitors, microphones, transducers for ferroelectric materials, storage in tapes or hard drives and information processing application for ferromagnetic materials. And the elements generating for ferroelectric and ferromagnetic materials is shown in Figure 2.3 [3,15,16]. In Figure 2.3, the elements which are used to fabricate ferroelectric and ferromagnetic are in the transition element group based on lead (Pb) or bismuth (Bi) elements.
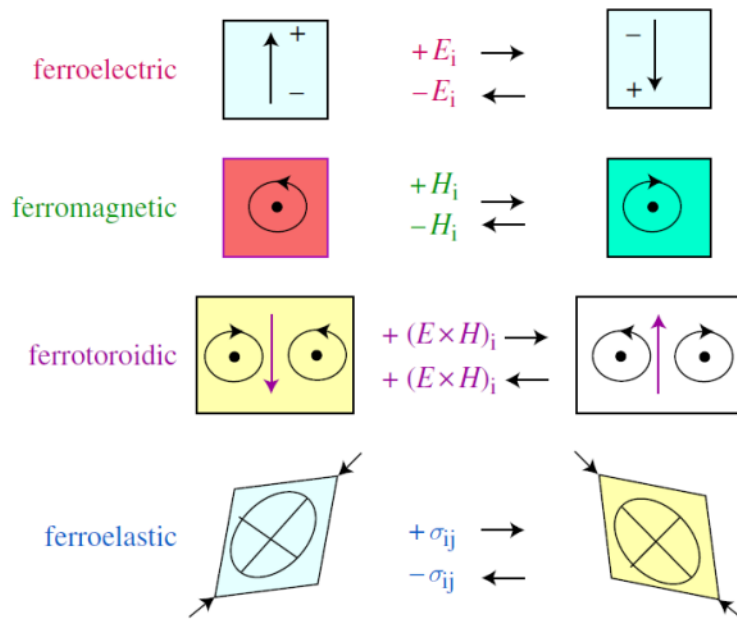

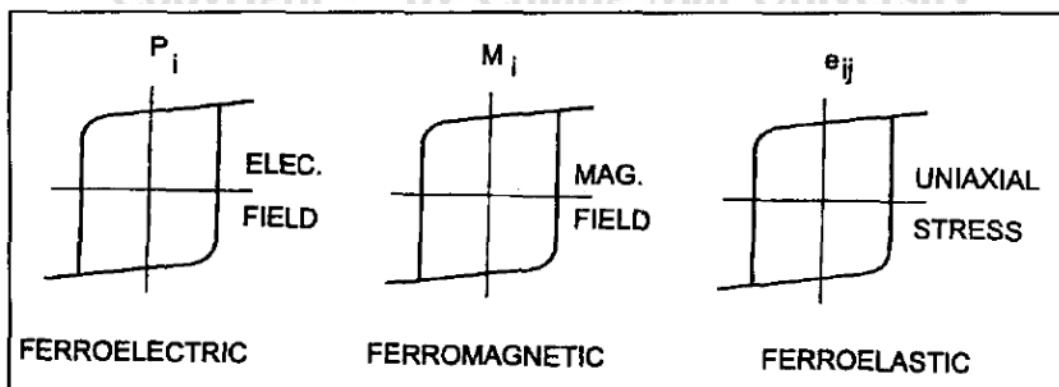Figure 2.1 Schematic of the ferroic orders, conjugated fields and corresponding symmetry operations [15]

Figure 2.2 Typical hysteresis loops for ferroelectrics P(E), ferromagnetics M(H) and ferroelastics $e_{ij}(\sigma)$ [3]
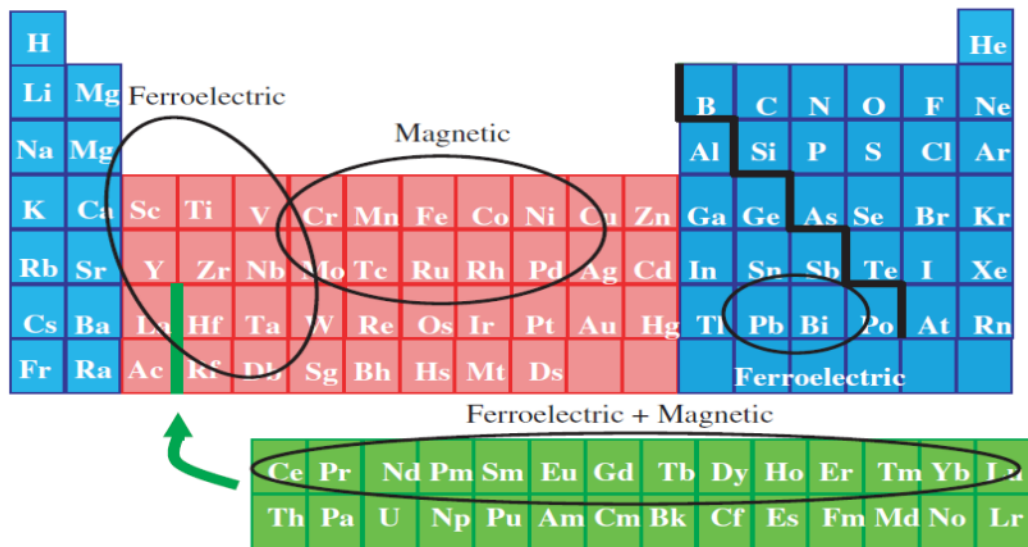
Figure 2.3 Periodic table of the elements highlighting the elements generating magnetic and ferroelectric behavior [16]

2.1.1 Ferroelectric materials and applications

Ferroelectric materials are the materials which possess ferroelectric phase, a state of spontaneous polarization (P_s) domain which the reorientation is affected by electric field, shown as hysteresis of polarization in Figure 2.4 and are the subclasses of functional dielectrics as shown in Figure 2.5. In Figure 2.4, the hysteresis of spontaneous polarization is shown when ferroelectric materials are affected by electrical field, more effective energy is used to switch the spontaneous polarization called coercive field (E_c) then causes fully switching of spontaneous polarization called saturate polarization (P_s) at the maximum high electric field and when the electrical field is turned off to zero field; this remains some of switching spontaneous polarization called remnant polarization. Figure 2.5 shows the subclass of dielectric materials which materials generate couple of charge affected by effective field; piezoelectrics are related to stress, pyroelectrics are related to heat; and ferroelectrics are related to spontaneous polarization caused by asymmetry structure which is reversed and shows hysteresis of polarization and strain by electrical field. Ferroelectric materials have been used in many applications such as memories, capacitors, sensors/actuators and optical devices

9

because of wide useful properties of them in ferroelectric hysteresis, high permittivities, piezoelectric effect, pyroelectric effect and advance in electro-optic effect. All properties results from non-centrosymmetric structure of ferroelectric materials at the temperature lower than Curie temperature, according to induced spontaneous polarization inside ferroelectric materials when ferroelectric materials cooling down from paraelectric phase to ferroelectric phase at Curie temperature or phase transition temperature. And the spontaneous polarization domains are oriented when subjected to electrical fields to induce the strains of ferroelectric materials, or generated electrical energy when ferroelectric materials are subjected to the stress due to spontaneous polarization domains are oriented [1,4,17].
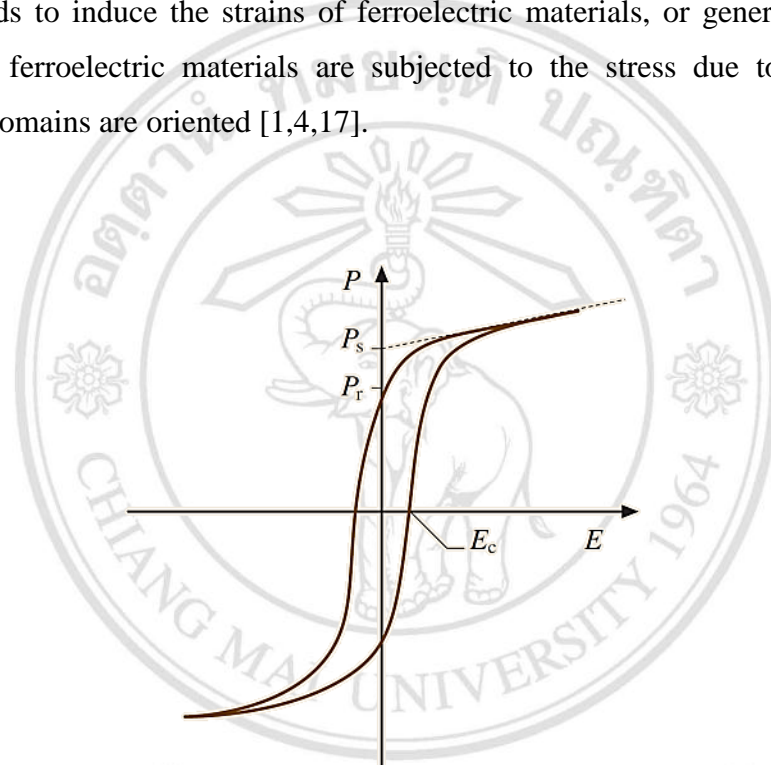
Figure 2.4 Ferroelectric hysteresis loop- spontaneous polarization (P_s), remanent polarization (P_r), coercive field (E_c) [18]
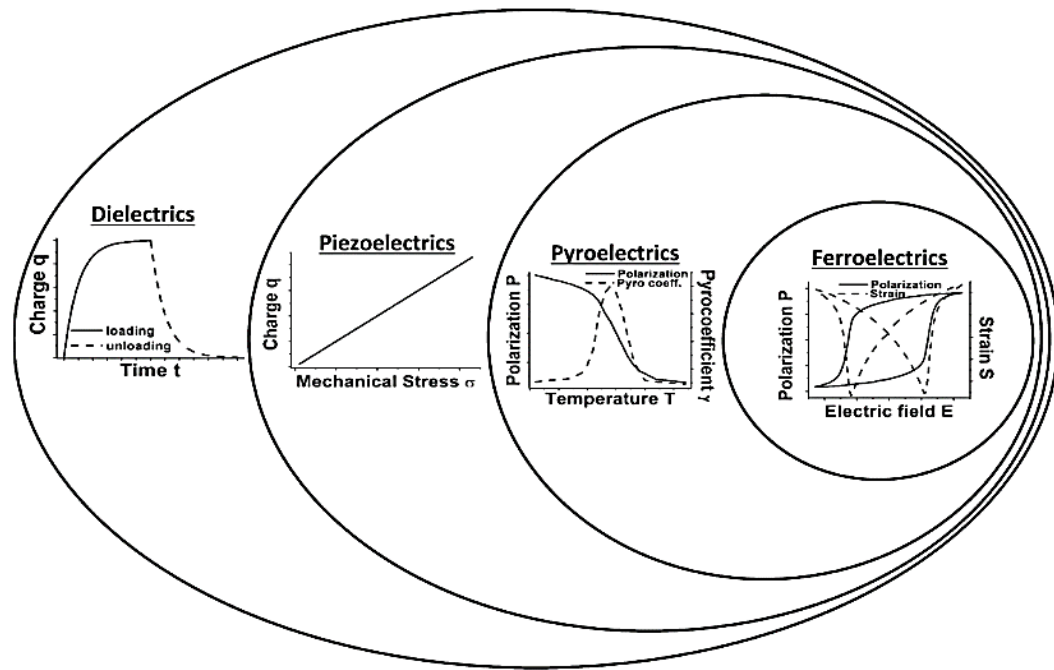
10

Figure 2.5 Ferroelectric is the subclasses of functional dielectrics [19]

Most of useful ferroelectric materials such as lead lanthanum zirconate titanate (PLZT) in electrooptic devices, lead magnesium niobate – lead titanate (PMN-PT) and lead magnesium niobate – lead zirconate titanate (PMN-PZT) in actuator applications, are perovskite-type structure which the structure was discovered as recently as 1921 in Rochelle salt by Valasek. The perovskite-type structure has ABO_3 formula where A and B are cations based on a cubic close-packed with the A-ion coordinated with 12 oxygen ions and the B-ion in the octahedral interstices as shown in Figure 2.6(a), and shows cubic closed-packed (hexagonal) which B are placed between two adjacent AO_3 layers as shown in Figure 2.6 (b). At temperature above Curie temperature, perovskite-type structure exhibiting centrosymmetric cubic structure, all ions are in equilibrium position which A^{2+} ions at the cube corners, O^{2-} ions at the face centers and B^{4+} ion at the body center as shown in Figure 2.7(a). But at below Curie temperature, perovskite-type structure exhibiting non-centrosymmetric structure, tetragonal structure for $BaTiO_3$, and spontaneous polarization is induced according to a slightly deformed, with A^{2+} and B^{4+} ions displaced relative to the O^{2-} ions, thereby creating a dipole as shown in Figure 2.7(b) [17].
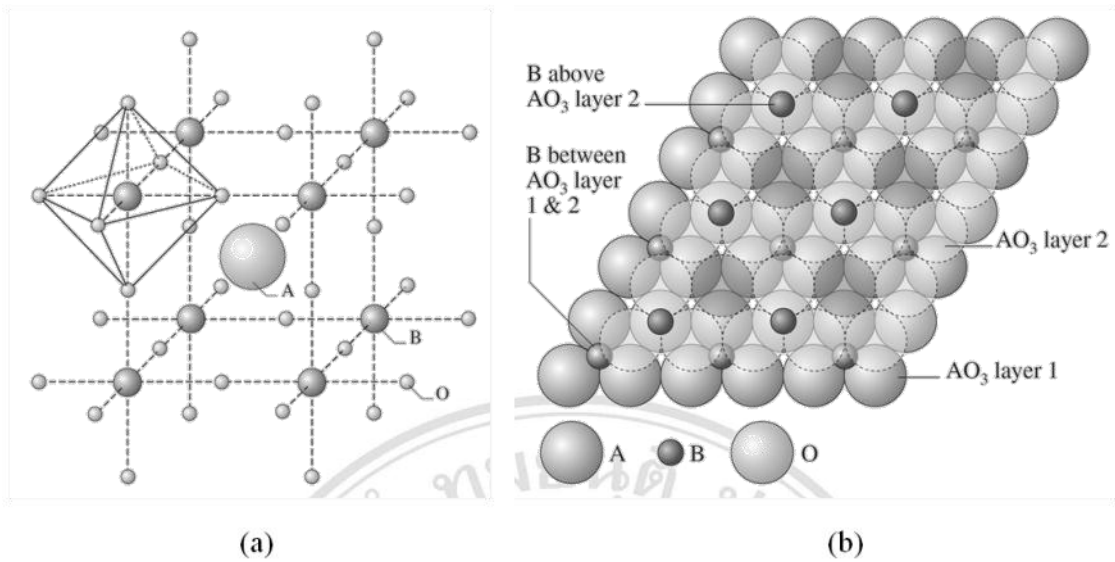
11

Figure 2.6 (a) The perovskite type structure and (b) closed-packed layer of perovskite type structure [8]
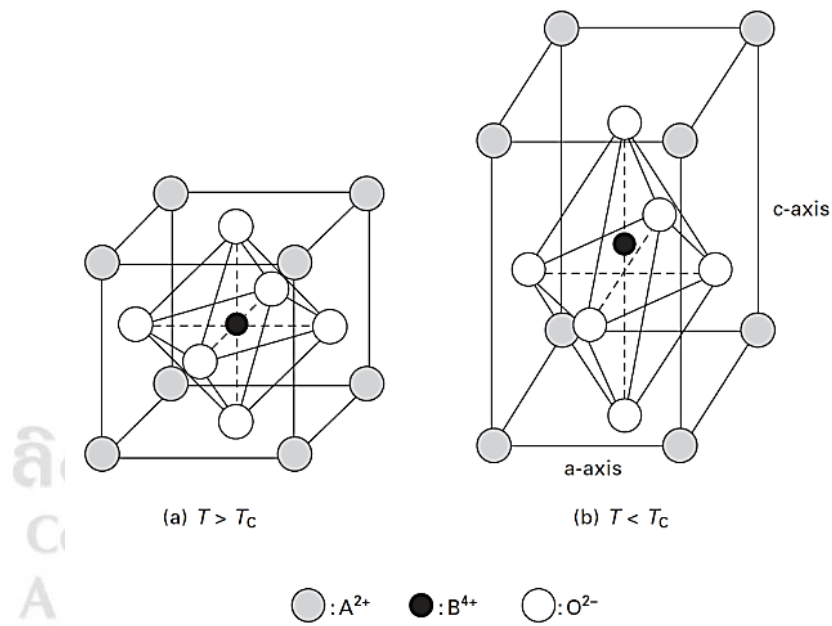

Figure 2.7 Perovskite structure (a) above (b) below Curie temperature of BaTiO$_3$ [20]

2.1.2 Piezoelectricity and electrostriction

Two characters of the induced strain exhibit when insulating materials are subjected to electrical field. First the converse piezoelectric effect, the linear relation of induced strain is caused by electric field as shown in Figure 2.8(a). Second the electrostriction phenomena, the nonlinear relation or quadratic behavior of induced strain caused by electric field as shown in Figure 2.8(b). Examples of piezoelectric materials are PLZT and BST materials in Figure 2.8(c), which was useful in many commercial applications such as pressure and acceleration sensors, piezo-vibrators precision positioners, pulse drive linear motors and ultrasonic motors [1]. An example of electrostrictive materials is PMN-PT relaxor ferroelectric material in Figure 2.8(c), which was useful in many commercial applications such as actuators and ultrasonic transducers [1]. And the equation of piezoelectric and electrostriction can be written in tensor form as [1,4];

$$s_{ij} = d_{ijk}E_k + M_{ijkl}E_kE_l \qquad (2.1)$$

where s_{ij} is induced strain; E_k and E_l are components of electric field; d_{ijk} is the piezoelectric tensor component and M_{ijkl} is the electrostriction tensor component.
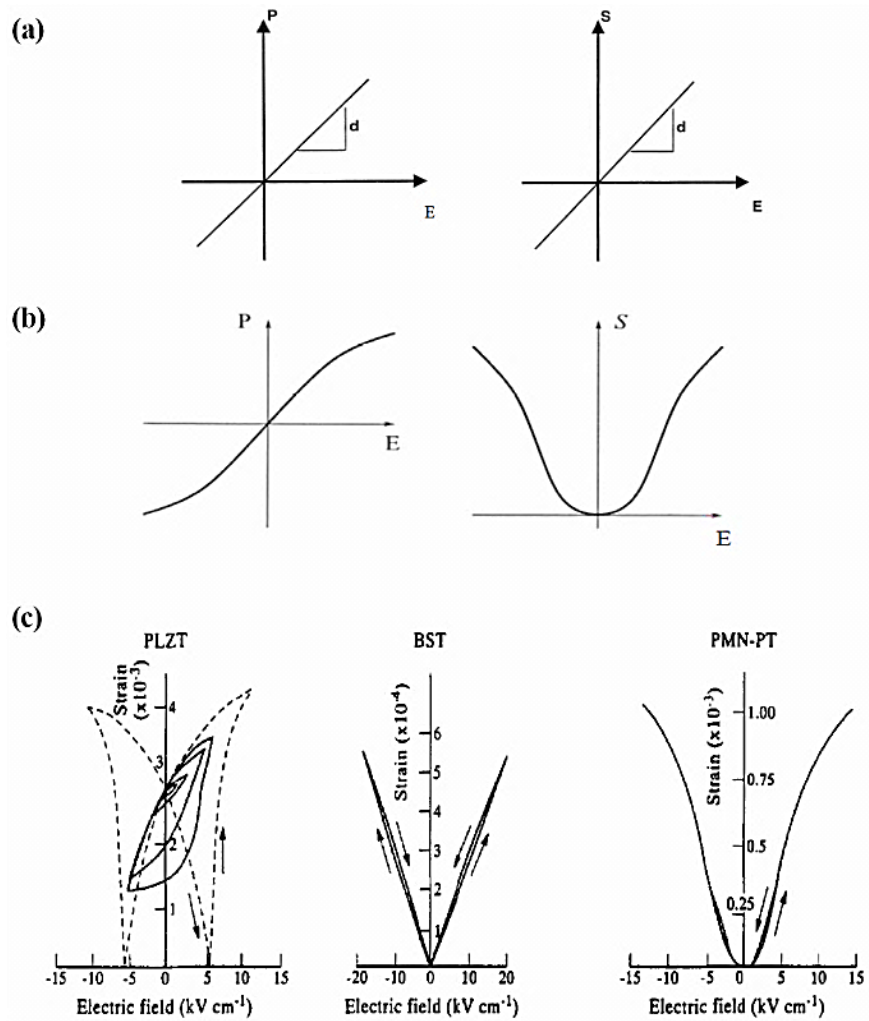
.

13

Figure 2.8 P-E and s-E graph of (a) Piezoelectric materials, (b) Electrostrictive

materials, (c) PLZT, BST and PMN-PT [1,21,22]

For ferroelectric materials, the electric field induced strain is caused by spontaneous polarization inside as shown in Figure 2.9, the polarization and induced strain showed hysteresis loop behavior when bipolar electric field is applied seen as the electric field loop tracing from path number 1 to 7, the spontaneous polarization domains show non homogeneous direction at number 1 then affected by electric field and all domain are reoriented at the coercive field (E_c) to full switching saturate polarization (P_{sat}) or induced strain (S_{sat}) in the direction of applied electric field at number two and remain remnant polarizations at number tree. The same behavior is shown for polarization and induce strain affected by the minus electric field in number

14

path four to six. And the induced strain relation in equation (2.1) can be written as a function of polarization as [1,4];

$$s_{ij} = g_{kij}P_k + Q_{ijkl}P_kP_l \tag{2.2}$$

where s_{ij} is induced strain; P_k and P_l are components of electric field; g_{ijk} is the piezoelectric tensor component and Q_{ijkl} is the electrostriction tensor component.

In nonlinear term in ferroelectric phase as shown in Figure 2.9, the polarization (P) was possessed by spontaneous polarization (P_s) and electric field (E), so the induced strain equation can be written as [1];

$$P = P_s + \varepsilon_0\varepsilon E^2 \tag{2.3}$$

$$s = Q(P_s + \varepsilon_0\varepsilon E)^2 \tag{2.4}$$

where ε_0 is the dielectric permittivity and ε is the relative permittivity

For high spontaneous polarization of ferroelectric materials, the induced strain was mainly possessed by spontaneous polarization as shown in Figure 2.9, and the induced strain equation (2.4) can be written as [1,23];

$$s = QP_s^2 \tag{2.5}$$

The deformation in ferroelectric materials can be classified into two types, which are 180° domain reversal such as lead titanate PT, soft and hard lead zirconate titanate PZT exhibit tetragonal structure in normal ferroelectric phase. And 90° domain reorientation materials are lead magnesium niobate – lead titanate PMN-PT, lead magnesium niobate – lead zirconate titanate PMN-PZT, and lead lanthanum zirconate titanate PLZT exhibit rhombohedral or mixed structure at MPB in relaxor ferroelectric near paraelectric phase. In Figure 2.10, lead titanate PT shows tetragonal structure in ferroelectric phase at temperature lower than Curie temperature (T_c), the spontaneous polarization was changed as 180° domain reversal and 90° domain reorientation when affected by electric field and stress respectively. Associated with Figure 2.11, the

15

volume fraction of domain as a function of electric field of PZT shows 90° domain reorientation (contributes to induced strain) and switches before 180° domain reversal (contributes to polarization) at position G and I respectively [1]. And when the induced strain plotted as a function of polarization was showed hysteresis and slimmer loop due to 180° domain reversal in transverse and parallel of $Pb(Ni_{1/3}Sb_{2/3})O_3$-$PbTiO_3$-$PbZrO_3$ and 90° domain reorientation in transverse of PMN-PT relaxor ferroelectric as shown in Figures 2.12 and 2.13 respectively.
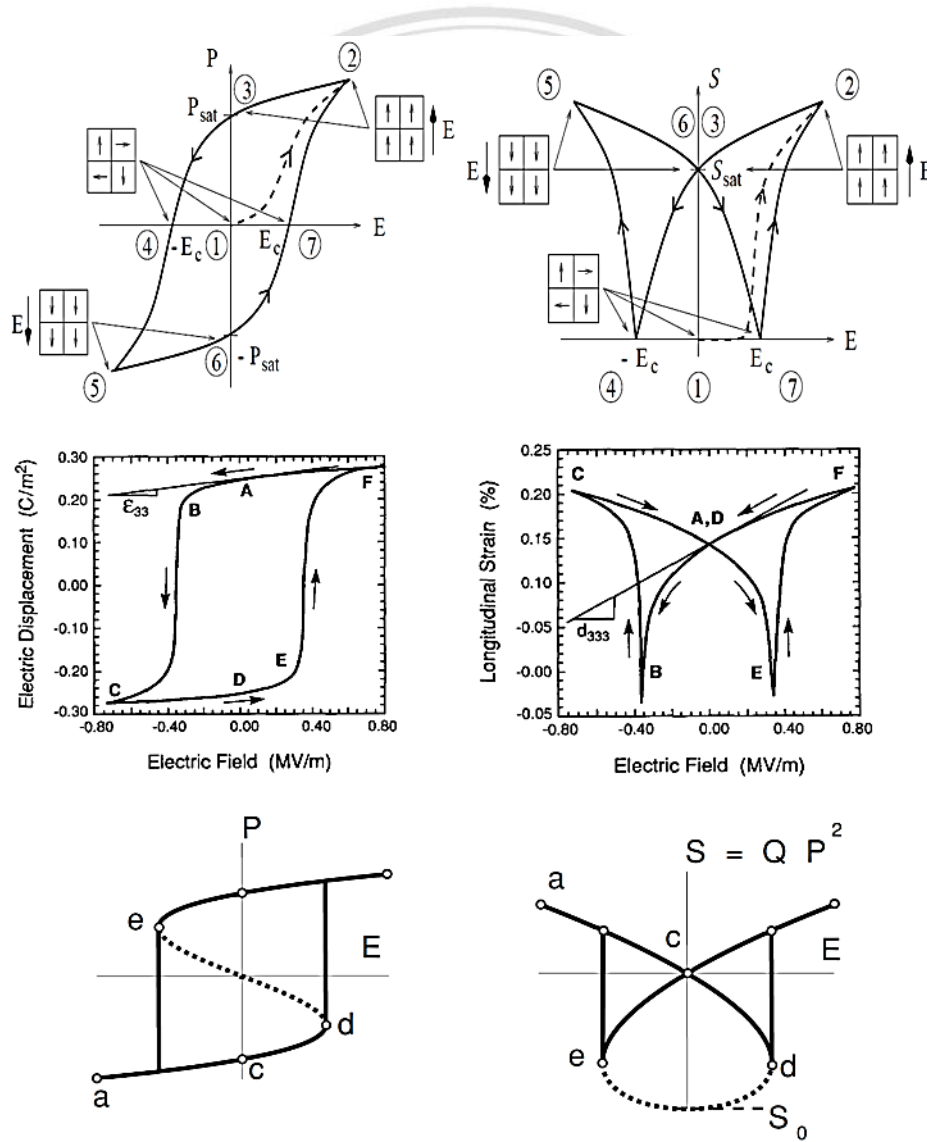
Figure 2.9 Relation of spontaneous polarization and induced strain of ferroelectric

materials [22-25]
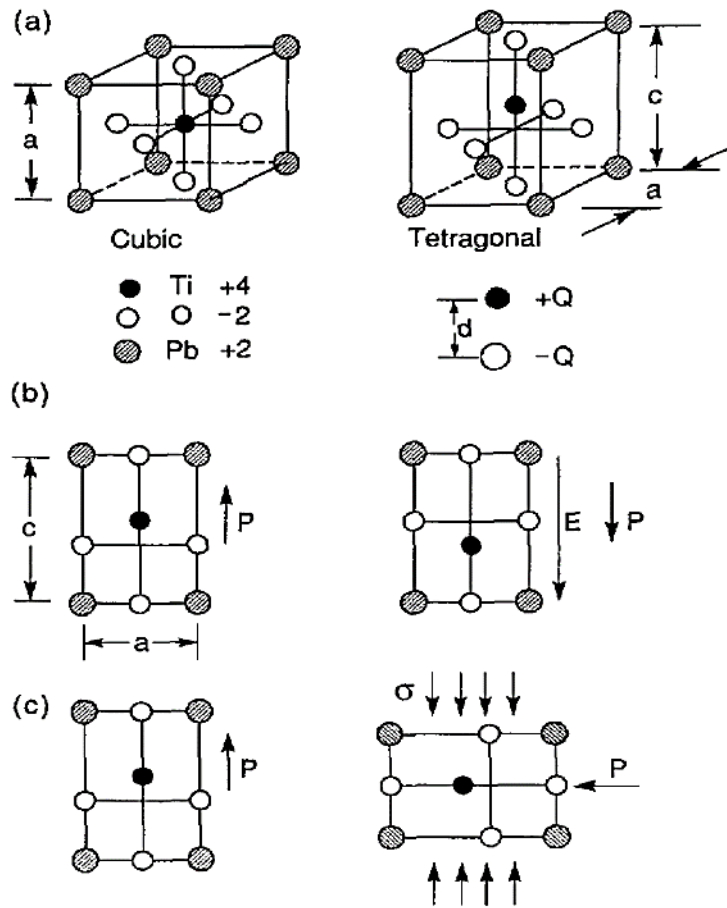
Figure 2.10 (a) Tetragonal of PT structure and (b) 180° and (c) 90° domain reorientation
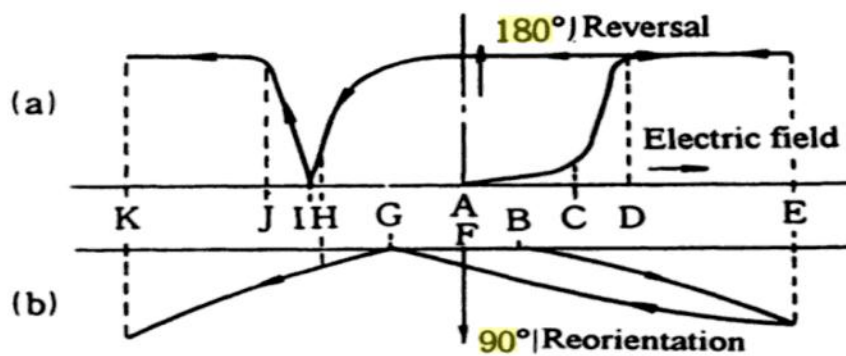in ferroelectric phase [24,25]

Figure 2.11 180° domain reversal and 90° domain reorientation as a function of electric
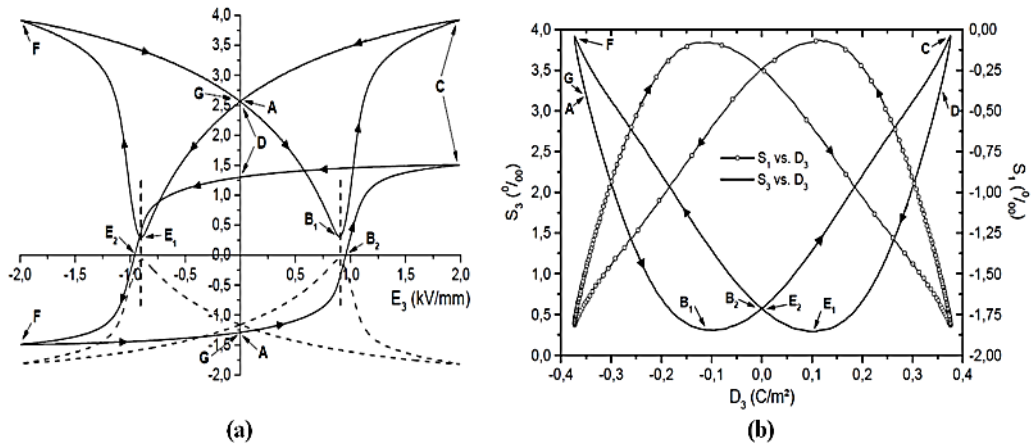field [1]

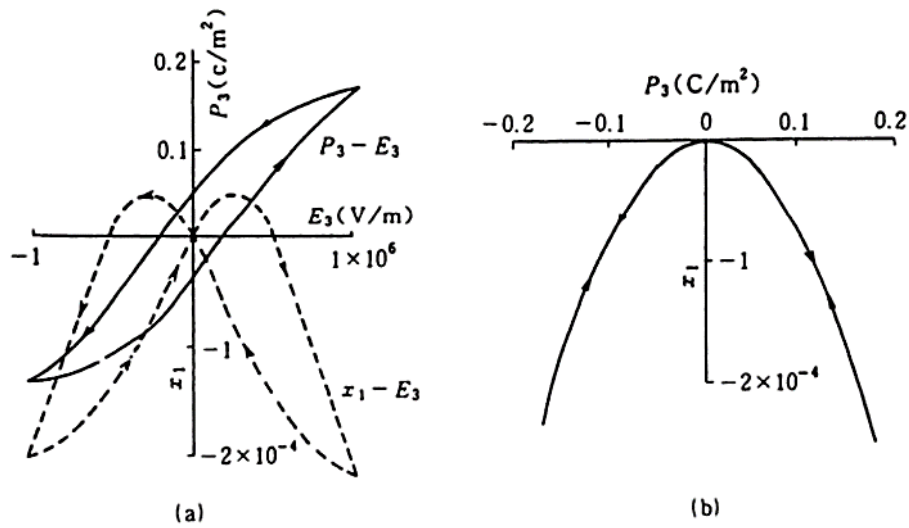Figure 2.12 180° domain reversal of $Pb(Ni_{1/3}Sb_{2/3})O_3$-$PbTiO_3$-$PbZrO_3$ [21]

Figure 2.13 90° domain reorientation of PMN-PT [1]

2.1.3 Temperature dependent behavior

Temperature dependent behavior of ferroelectric materials is associated with transition of phase/structure and lattice parameter expansion affected by the temperature change. For example, ferroelectric material $BaTiO_3$ exhibited cubic structure in paraelectric phase above Curie temperature at 130°C, when the temperature is down to 0°C, -90°C and below -90°C the structure is developed to tetragonal, monoclinic and rhombohedral, all are ferroelectric phase as shown in Figure 2.14, corresponding to the

lattice expansion with temperature as shown in Figure 2.15, the average lattice parameter was increases as a function of temperature increased due to the displacement of atomic ions at affected temperature [17].
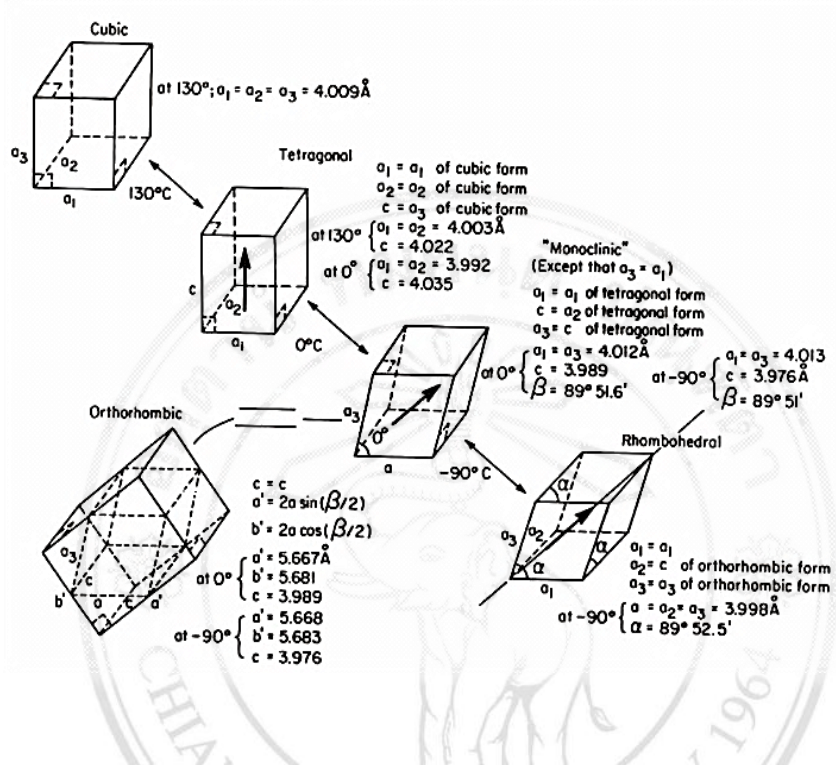

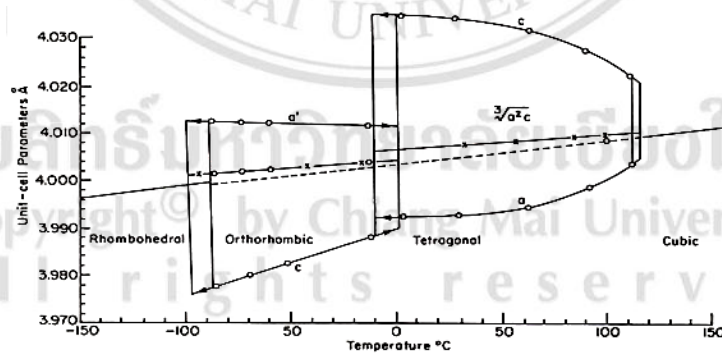Figure 2.14 Phase transition with temperature of $BaTiO_3$ [26]

Figure 2.15 Lattice parameters expansion with temperature of $BaTiO_3$ [17,27]

The temperature dependence of ferroelectric materials affects the electric field induced strain and polarization behavior and the induced strain as a change of polarization which means spontaneous polarization mainly controls ferroelectric

19

displacement, for example soft PZT temperature dependence is shown in Figure 2.16 (a) and (b). Soft PZT shows high spontaneous polarization with mainly 180° domain dominated in normal ferroelectric at lower temperature 19°C, and then both polarization and induced strain were decreased to slimmer less spontaneous polarization and transition to paraelectric phase when temperature was increased to 186°C. Figure 2.16(c) shows quadratic relation of induced strain and polarization at all temperatures.
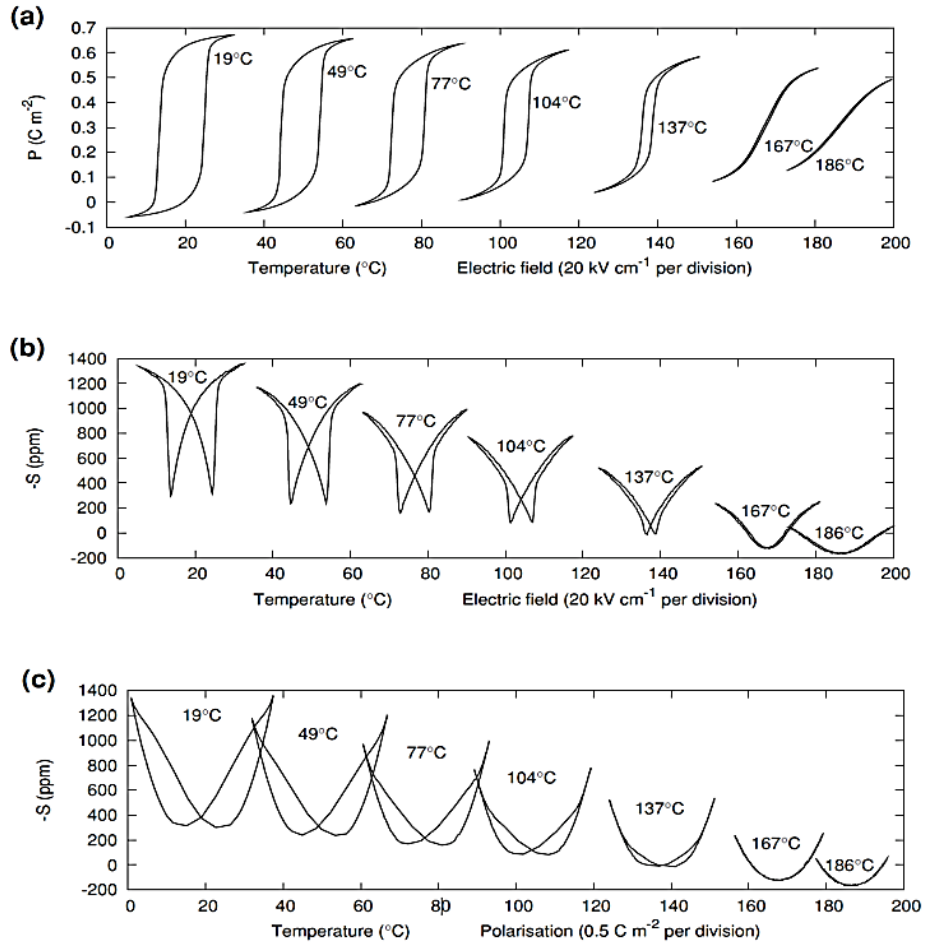
Figure 2.16 (a) polarization, (b) induced strain as a function of electric field and (c) induced strain as a function of polarization at different temperatures [23]

In 2011, Rauls and coauthors measured the full hysteresis loop for the relaxor ferroelectric 8/65/35 PLZT as a function of temperature. The electric field induced strain and polarization with butterfly shape curve and hysteresis loops at 25°C in ferroelectric phase changed to non-hysteresis quadratic electrostrictive behavior at 98°C

in paraelectric phase. The measured strain was plotted as a function of polarization for each temperature, the results showed a quadratic relationship [28].
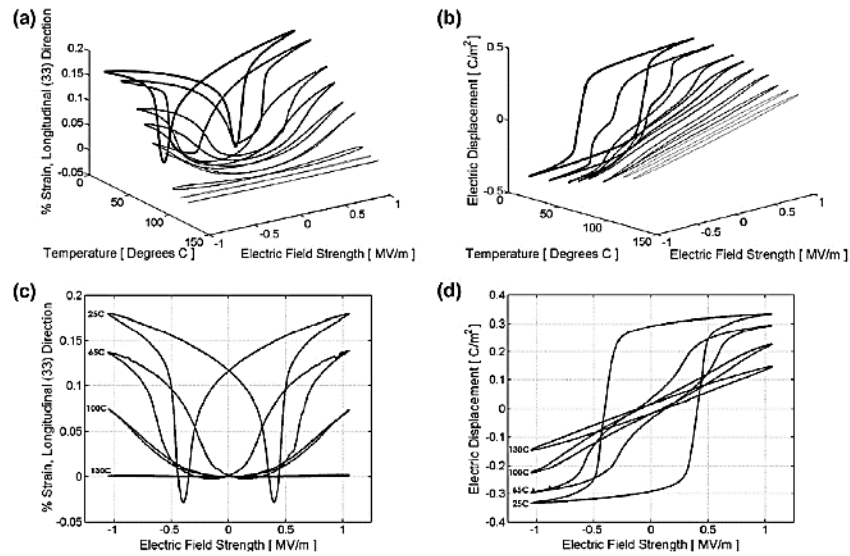

Figure 2.15 Induced strain and polarization as function of electric field at various temperatures [28]
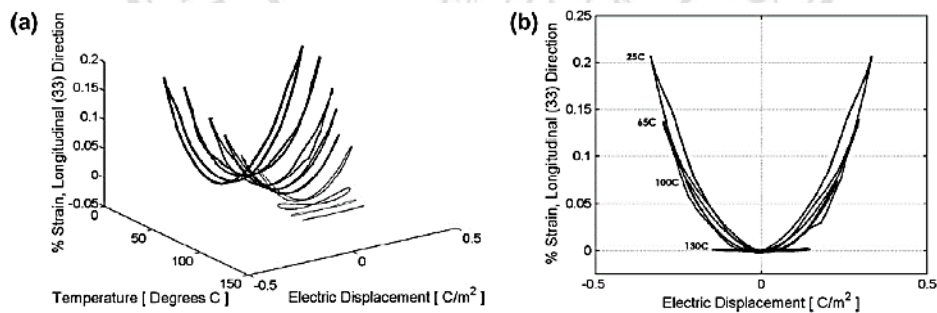
Figure 2.16 Induced strain as function of polarization at various temperature [28]

Another report in 2011, Tran and coauthors presents the changed ferroelectric properties of $Bi_{1/2}(Na_{0.82}K_{0.18})_{1/2}TiO_3$ (BNKT) ceramics modified by $Sr(K_{1/4}Nb_{3/4})O_3$ (SKN), which exhibited induced strain behavior as functions of composition and temperature. Unmodified BNKT (x=0) maintained the butterfly shape curve of typical normal ferroelectric materials overall within the measured temperature range. In the

21

case of x=0.02, the sample showed a higher butterfly-shaped curve at 25°C but disappeared at 100°C. The less ferroelectric properties was shown in the case of x=0.05 all showed quadratic shape with electric field indicated near paraelectric phase as shown in Figure 2.17 [29].
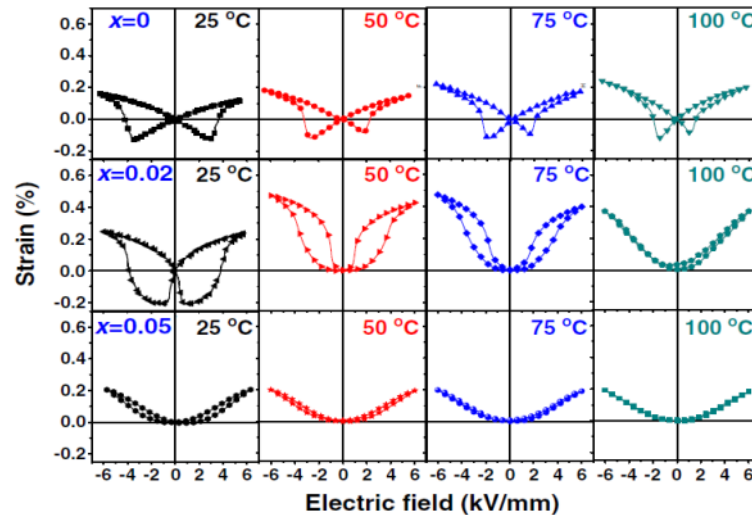

Figure 2.17 Temperature dependence of bipolar S–E hysteresis loop in (1–x)BNKT–xSKN ceramics where x=0, 0.02 and 0.05 [29]

2.1.4 Magnetoelectricity

Magnetoelectric effect is coupling between magnetic and electric variables as shown in Figure 2.18. An applied electric field not only induces electrical polarization but affects magnetization as well and vice versa [4,30]. After 1970, a wide range of devices used magnetoelectric effect such as modulation of polarizations, amplitudes and phases of optical waves, magnetoelectric data storage and switching, optical diodes, spin-wave generation, and composite materials of magnetostrictive and piezoelectric materials [31,32].
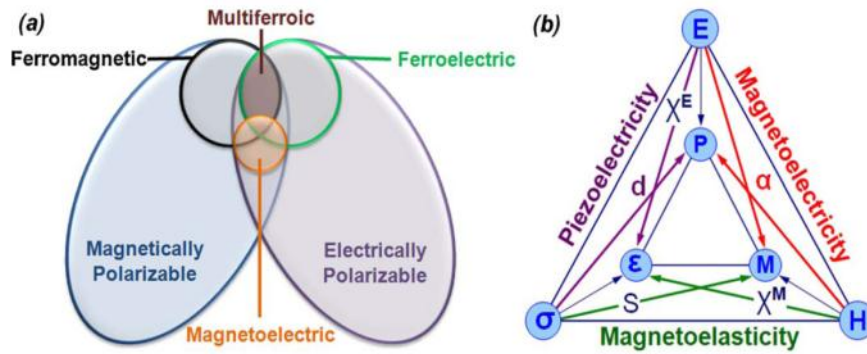
Figure 2.18 Multiferroic and magnetoelectric materials. (a) Relationship between multiferroic and magnetoelectric materials. (b) Schematic diagram illustrating different types of coupling present in materials [30-34]

In 2012, Liu and coworker presented the temperature and magnetic field dependencies of ferroelectric properties of $Au/BiFeO_3/La_{5/8}Ca_{3/8}MnO_3/SrTiO_3$ thin films. They found the decreased coercive electric field of $BiFeO_3/La_{5/8}Ca_{3/8}MnO_3$ (BFO/LCMO) when the magnetic fields were increased around the Curie temperature of LCMO (~220 K). And the remnant polarization P_r increased at 10 kHz of frequency. The variations of ferroelectricity were mainly related to the magnetoelectric-coupled interface between BFO and LCMO [35].
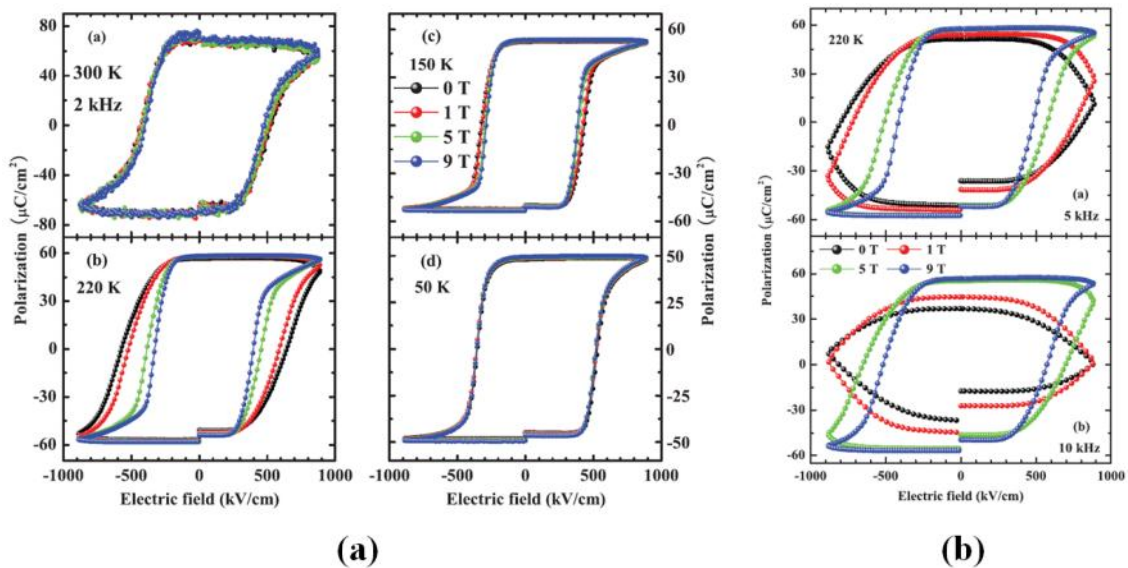

Figure 2.19 P-E hysteresis loops in magnetic fields of 0, 1, 5, and 9 T at (a) different temperatures (b) at 220 K [35]

In 2008, Bednarek described the production method of the elastic composite containing ferrous particles and titanium barium particles dispersed in the porous silicone matrix, ferromagnetic particles (p_f), ferroelectric particles (p_e) and porosity factor (p_p). The electrostriction of composite samples induced by the electric field with maximum intensity 1.5×10^6 V/m, also induced by the magnetostriction in the magnetic field with maximum induction 1 T was also investigated. The Michelson interferometer was applied in order to detect the change of sample elongation $\Delta l/l_0$. An interesting effect was a simultaneous impact on samples of the electric and the magnetic field. It appeared that the relative elongation of $\Delta l/l_0$ in this case was smaller than the sum of relative elongations caused by the electric and magnetic field separately [36].
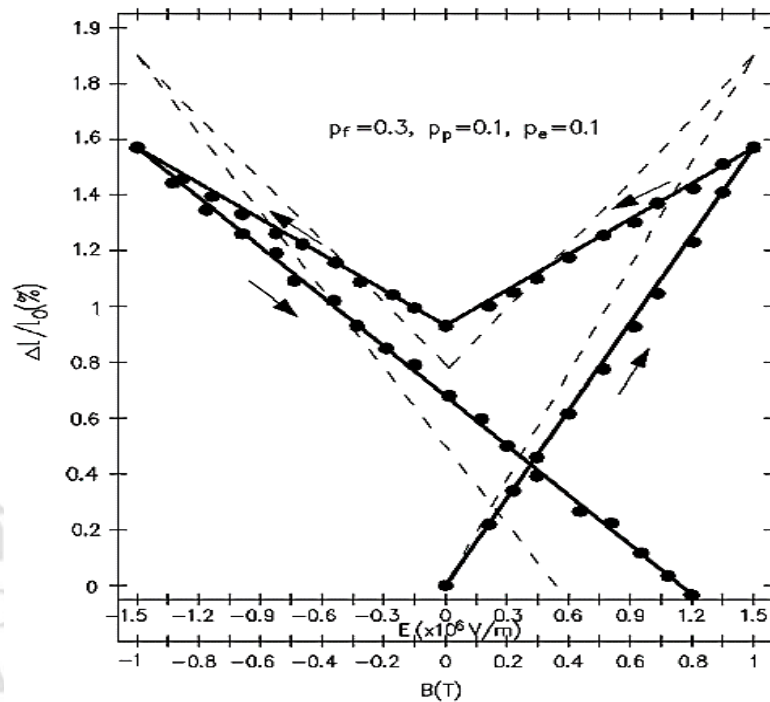

Figure 2.20 Relative elongation $\Delta l/l_0$ on simultaneous changes of electric field E and magnetic field B compared the elongation sum (dashed line) caused by separated changes of E and B of magnetorheological composite samples [36]

2.2 Michelson interferometer

Interference phenomena occur when radiation beam more than one path from its source to detection screen. It may be described as the resultant intensity at the point of detection [14]. Interferometers are classified as "two beams" or "multiple beams" according to the number of interfered beam. In our single beam interferometer based on the Michelson Interferometer, is necessarily classed in the "two beam" interferometer. The term "single" is referred to the single laser beam from sample surface. Single beam interferometers have been used by many researchers as a tool for measuring the piezoelectric and electrostrictive properties of materials (Luymes, 1983, Zhang et al., 1988, Meng et al., 1988, Li et al., 1995, and Sundar, 1996) [12].

Michelson interferometer is classified as amplitude division of two monochromatic wave interference [37,38], and it is long time well known for small displacement in resolution about 10^{-14} m [12,13] depending on measurement set up. Michelson interferometer set-up is shown in Figure 2.21, the coherence monochromatic laser beam from stable He-Ne source is separated at beam splitter into two equal amplitude beams to reflect on mirror M_1 and M_2 then coming back to interfering on the screen. The interference fringe patterns in Michelson are divided into two types depending on the mirror alignment of each mirror as shown in Figure 2.22. First is circular fringe pattern where the mirror M_1 and M_2 are parallel to reflected the beams as shown in Figure 2.22(a). Second is localized fringe pattern where the two mirrors have difference in an angle plane to reflect the beams as shown in Figure 2.22(b) [39].
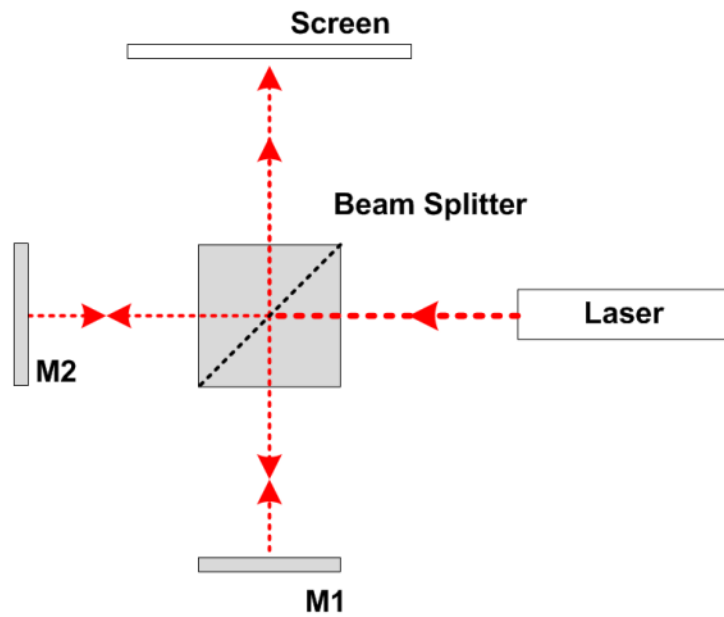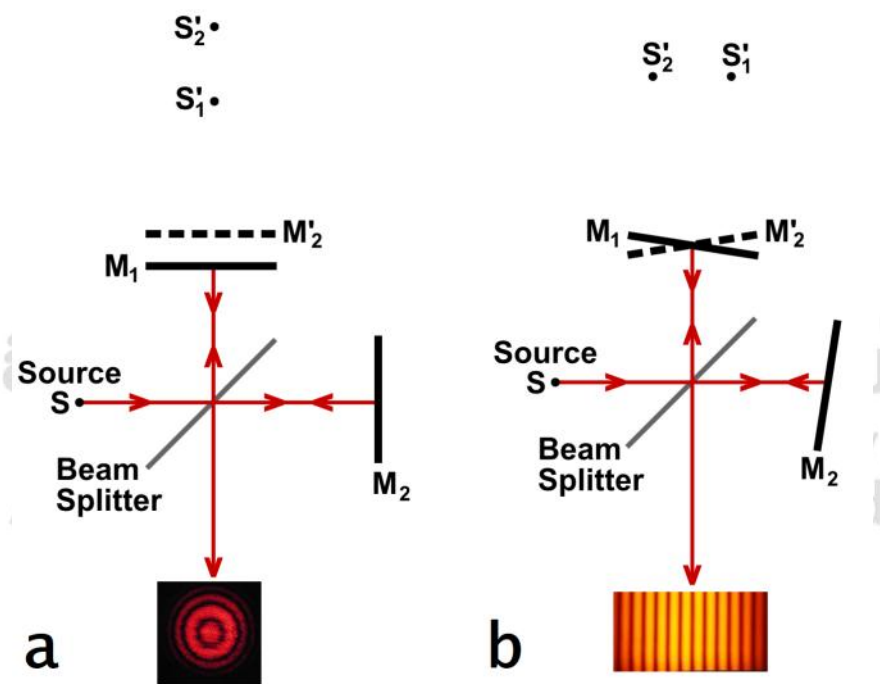
25

Figure 2.21 Michelson interferometer

Figure 2.22 Formation of fringe in Michelson interferometer (a) a circular fringe and (b) localized fringe [39]

When two monochromatic lights superimpose, the interference pattern intensity can be written as a superimposed function of complex wave as expressed in equation (2.6) [37-41].

$$E_C = E_A + E_B \tag{2.6}$$

where $E_A = E_{0A}\exp(-i(\omega t - kr_A + \delta_A))$ and $E_B = E_{0B}\exp(-i(\omega t - kr_B + \delta_B))$

And interference intensity of two light is

$$I = |E_C|^2 \tag{2.7}$$

$$I = \left|(E_A + E_B)(E_A^* + E_B^*)\right|$$

$$I = \left| \begin{array}{l} \left[E_{0A}\exp(i(kr_A - \delta_A)) + E_{0B}\exp(i(kr_B - \delta_B))\right] \\ \times\left[E_{0A}\exp(i(kr_A - \delta_A)) + E_{0B}\exp(i(kr_B - \delta_B))\right] \\ \times\exp(-i(\omega t))\exp(i(\omega t)) \end{array} \right|$$

$$I = \left(\begin{array}{l} E_{0A}^2 + E_{0B}^2 + E_{0A}E_{0B}[\exp(ik(r_A - r_B) - (\delta_A - \delta_B)) \\ + \exp(ik(r_B - r_A) - (\delta_B - \delta_A))] \end{array} \right)$$

$$I = E_{0A}^2 + E_{0B}^2 + 2E_{0A}E_{0B}\cos\delta$$

$$I = I_{0A} + I_{0B} \pm 2\sqrt{I_{0A}I_{0B}}\cos\delta \tag{2.8}$$

$$I = 2I_0 + 2I_0\cos\delta$$

$$I = 4I_0\cos^2(\frac{\delta}{2})$$

And the phase difference (δ) of the source at same frequency is related to the path difference (Λ) as;

$$\delta = 2\pi\Lambda / \lambda$$

27

The maximum and minimum of interference intensity can be evaluated from equation (2.8) which depends on phase difference (δ) of the two interference beams can be written as [38]

$$I_{max} = I_{0A} + I_{0B} + 2\sqrt{I_{0A}I_{0B}}$$

$$I_{min} = I_{0A} + I_{0B} - 2\sqrt{I_{0A}I_{0B}}$$

then the visibility ν of this interference is

$$\nu = \frac{I_{max} - I_{min}}{I_{max} + I_{min}}$$

The path difference of mirror M_1 and M_2 in Michelson interferometer setup when source (S) reflected though the two mirrors then recombine on the screen, which the path difference (Λ) can be written as in equation (2.9)

$$\Lambda = 2d cos\theta \tag{2.9}$$

which

$$2d cos\theta = m\lambda \tag{2.10}$$

where there are bright fringes when $m = 0, 1 ,2, ...$ and dark fringes when $m = \frac{1}{2}, \frac{3}{2}, \frac{5}{2}, ...$ [37].

28